Geomechanics and Engineering, *Vol. 17, No. 4 (2019) 323-331*
DOI: https://doi.org/10.12989/gae.2019.17.4.323

Experimental study of crack propagation of rock-like specimens containing conjugate fractures

Wenbin Sun*[1,2], Houqian Du[1], Fei Zhou[1] and Jianli Shao[1]

[1]State Key Laboratory of Mining Disaster Prevention and Control, College of Mining and Safety Engineering, Shandong University of Science and Technology, Qingdao 266590, People's Republic of China
[2]Key Laboratory of Modern Mining Engineering, AnHui Province (Anhui University of Science and Technology), Huainan, 232001, People's Republic of China

(Received November 21, 2018, Revised February 18, 2019, Accepted February 19, 2019)

Abstract. The presence of defects in nature changes the physical parameters of the rock. In this paper, by studying the rock-like specimens with conjugated fractures, the horizontal angle and length are changed, and the physical parameters and failure modes of the specimens under uniaxial compression test are analyzed and compared with the results of simulation analysis. The experimental results show that the peak strength and failure mode of the rock-like specimens are closely related to the horizontal angle. When the horizontal angle is 45°, the maximum value is reached and the tensile failure mode is obtained. The fracture length affects the germination and propagation path of the cracks. It is of great significance to study the failure modes and mechanical properties of conjugated fracture rock-like specimens to guide the support of fractured rock on site.

Keywords: rock-like material; conjugate fractures; failure mode; uniaxial compression; cracks propagation

1. Introduction

Naturally occurring rock masses are heterogeneous anisotropic discontinuous composite structures composed of a large number of defects such as joints, fractures, interlayers, and weak surfaces. The difference between this type of defective rock and the general homogeneous rock mass is that the defect controls the rock damage and deformation (Bagheripour *et al*. 2011, Erarslan 2016, Komurlu *et al*. 2016, Shen and Barton 2018, Zhou *et al*. 2015). Intensive study of fractured rock masses provides guidance for the construction of underground geotechnical engineering.

Experimental study in the laboratory is an important tool to observe and analyze the failure of defective specimens. The fractures length and angle have a great influence on the mechanical properties of specimens under uniaxial compression. The failure mode and crack propagation are closely related to the geometry of the fracture (Panaghi *et al*. 2015, Sun *et al*. 2018). Under triaxial compression, the variation of peak strength and residual strength of the specimens was studied via varying confining pressure. It was concluded that confining pressure is an important factor affecting the failure mode of the specimens (Mohammadi and Tavakoli 2015). The strength variation and failure modes of rock specimens with fracture under uniaxial tension are related to the geometric characteristics of fracture dip angle, fracture spacing and fracture width. When the length of the rock bridge is smaller than the fracture length, the failure is caused by the joint action of single and multiple fractures (Yang *et al*. 2013). Experimenting with different loading rates, the number of cracks, the strength of specimens and the change of initial crack formation during the failure process of cracked rock are studied. The change of loading rate has a great influence on the failure and instability of rock. By comparing the crack propagation mode and strength change under different loading rates, the failure mechanism of rock under dynamic loading is analyzed (Cai *et al*. 2019, Kong *et al*. 2018, Wang *et al*. 2017).

Numerical simulation is not only a verification of experimental results, but also a supplement to experimental study. Fu *et al*. (2017) simulated the failure modes of rock mass with fractures under uniaxial and biaxial loading by FLAC3D. The authors compared the progressive failure process of rock specimens with two fractures, and analyzed the crack propagation and stability of a slope project. Da Silva and Einstein (2013) and Yang *et al*. (2013) used FROCK to simulate the failure modes and mechanical properties of specimens with fractures under uniaxial compression and uniaxial tension, respectively. The authors compared simulation results with experimental results and the consistencies between them were obtained. Wang *et al*. (2014) used RFPA3D to analyze the evolution of cracks in three-dimensional space. The uniaxial compressive strength and fracture evolution mechanism of the two kinds of defect specimens with different fracture angle and rock bridge angle were analyzed. The most used monitoring methods are stress changes and displacement changes, which are observations and analysis of the external macroscopic of the specimens. Zhao *et al*. (2015) and Cao *et al*. (2017) used acoustic emission monitoring data combined with stress-strain curves to analyze the crack initiation, propagation,

*Corresponding author, Associate Professor
E-mail: swb@sdust.edu.cn

ISSN: 2005-307X (Print), 2092-6219 (Online)

polymerization process of the specimens with defects, as well as the location of internal cracks in the specimen. Lu *et al*. (2015) used CT scanning imaging technology to identify the positions inside fracture-containing specimens under uniaxial compression. The authors analyzed failure mode and crack propagation.

Both geometric shape and spatial position of the defects contained in the specimen have an important influence on the mechanical characteristics and failure modes of the specimen. The existing defect geometry and spatial position are mostly single fracture, parallel multiple sets of fractures (Haeri *et al*. 2015, Jin *et al*. 2017), parallel multiple sets of fractures and composite fractures (Zhou *et al*. 2015, Fu *et al*. 2017, Liu *et al*. 2017), non-parallel multiple sets of fractures (Lee and Jeon 2011, Haeri *et al*. 2014, Haeri *et al*. 2015, Zhang *et al*. 2015, Huang *et al*. 2016) and composite fractures (Yang *et al*. 2014, Wang and Tian 2018) have less research on cross-fractures (Sarfarazi *et al*. 2017, Zhou *et al*. 2018). There are few studies on cross-fractures. In this study, the failure mode and crack propagation of rock-like specimens under uniaxial compression experiments with different length and horizontal angle of two conjugate fractures are analyzed.

2. Manufacture and test method of rock-like specimen

2.1 Specimen material and preparation

The joints and fractures of the original rock are complex and cannot meet the requirements of the fracture shape for the purpose of this study. The rock-like materials can be used to obtain the required fracture shape on the basis of the mechanical properties of the original rock. Rock-like materials for the uniaxial compression test use high-strength gypsum powder as cementing material with appropriate amount of retarders and water reducers. The gypsum slurry used in the test is configured according to the gypsum-water mass ratio of 5.0:2.0. At room temperature, the mold release oil is applied to the outer surface of the fracture generating device and the inside of a metal mold with the size of 100 mm × 100 mm × 200 mm. The gypsum slurry is stirred in a stirrer for 1 min to be uniform, and then poured into a mold and vibrated by a vibration table. After the rock-like specimen was cured in the concrete curing box for 24 hours, the mold was removed and the fracture generating device was taken out. The curing was continued for 4 days. Mechanical parameters of rock-like specimens used in this study were measured by pouring a cubic specimen with a size of 70 mm under the same environmental condition. Mechanics parameters of the material are shown in Table 1.

The fracture in the rock-like specimen is generated by using a fracture generating device with a thickness of 1.5 mm placed in the metal mold before the gypsum slurry is poured into the mold. The length of the fracture generating device is the fracture length of the rock-like specimen fracture, as shown in Fig 1. The fractures length L is 50 mm and 60 mm respectively. The horizontal angle α is increased from 0° to 90° at an interval of 15°. In total, 21 sets of specimens were prepared. When the main fracture and the secondary fracture are the same, no difference was observed in the specimens. Hence, a total of 15 sets of specimens are sorted according to the test requirement number, as shown in Table 2.

Table 1 Material mechanics parameters of the specimens

Description	Value	Unit
Uniaxial compressive strength	14.4	MPa
Poisson's ratio	0.16	–
Elastic modulus	1.82	GPa
Density	1.48	g/cm^3

Table 2 Specimens sorting

Specimens	L_1/(mm)	L_2/(mm)	α/(°)
S01-S03	50	50	0(90)
S04-S06	50	50	15(75)
S07-S09	50	50	30(60)
S10-S12	50	50	45
M01-M03	50	60	0
M04-M06	50	60	15
M07-M09	50	60	30
M10-M12	50	60	45
M13-M15	50	60	60
M16-M18	50	60	75
M19-M21	50	60	90
H01-H03	60	60	0(90)
H04-H06	60	60	15(75)
H07-H09	60	60	30(60)
H10-H12	60	60	45

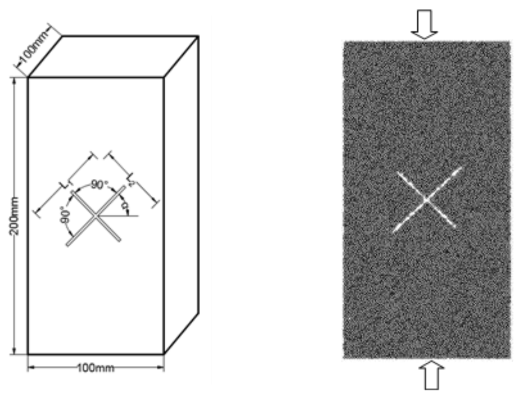

(a) Size diagram (b) Model diagram

Fig. 1 Model schematic diagram and PFC model diagram under uniaxial compression

2.2 Testing procedure

The uniaxial compression experiment was carried out on the high-precision microcomputer-controlled electro-hydraulic servo Shimadzu test machine in Shandong University of Science and Technology. During the experiment, the spindle was subjected to force-controlled loading at a speed of 0.02 mm/s. Butter was applied between the upper and lower ends of the specimen and the rigid bearing plate to weaken the influence of the end effect on the test results. A high-definition digital camera was used to record the fracture damage and crack development process for damage analysis.

3. Destructive strength and deformation behavior

3.1 Stress-strain relationships

The stress-strain curves of rock-like specimens under uniaxial compression are shown in Fig 2. The strength of rock specimens with conjugated fractures is lower than that of complete specimens. Significant difference in the stress-strain curves and mechanical parameters for rock specimens with conjugated fractures is observed for those with different horizontal inclination angles and fracture lengths. It shows that the horizontal inclination angles and fracture length have a significant effect on the mechanical properties of rocks with conjugated fractures.

The stress-strain curves of rock specimens with conjugated fractures under uniaxial compression show nonlinear characteristics compared with the complete specimens in the compaction stage in the first place and then the elastic stage. The stress is approximately linear with the strain growth, and the process is substantially shortened compared with the complete rock specimens. In the process of entering the plastic stage, the failure stress reaches the peak as the strain increases, which is significantly lower than that of the complete rock specimen. Once the stress peak enters the friction stage, the stress-strain curves drop rapidly, indicating the brittleness of the rock-like specimens.

With the increase of the horizontal angle α, the main fracture L_1 becomes horizontal from vertical to loading direction. At the same time, the secondary fracture L_2 becomes vertical from horizontal to loading direction. The peak stress of rock-like specimen under uniaxial compression increases first and then decreases, as shown in Fig 3. In addition, it can be found that the peak strength intensity increases and then decreases with the increase of the horizontal angle α for specimens group S. It reaches a maximum value of 3.64 MPa when the horizontal angle α is 45°. When the horizontal angle α increases from 0° to 45°, the peak strength intensity increased from 3.02 MPa to 3.64 MPa (20.5% increases). The peak strength intensity increases and then decreases with the increase of the horizontal angle α for specimens group M. It reaches a maximum value of 3.524 MPa when the horizontal angle α is 60°. When the horizontal angle α increases from 0° to 60°, the peak strength intensity increased from 2.91 MPa to 3.52 MPa (20.9% increases). The peak strength increases and then decreases with the increase of the horizontal angle α for specimens group H. It reaches a maximum value of 3.23 MPa when the horizontal angle α is 45°. When the horizontal angle α increases from 0° to 45°, the peak strength intensity increased from 2.66 MPa to 3.23 MPa (21.5% increases). The peak strength decreases with the increase of the fracture length under the same horizontal angle α. The peak strength increases at first and then decreases with the increasing horizontal angle α for the same main fracture.

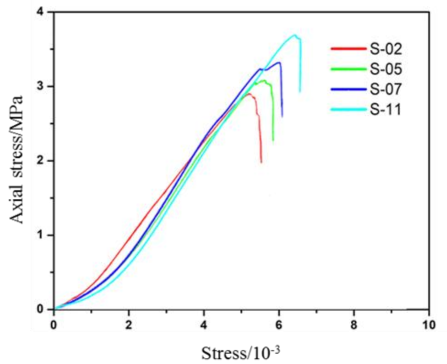

(a) Specimens group S

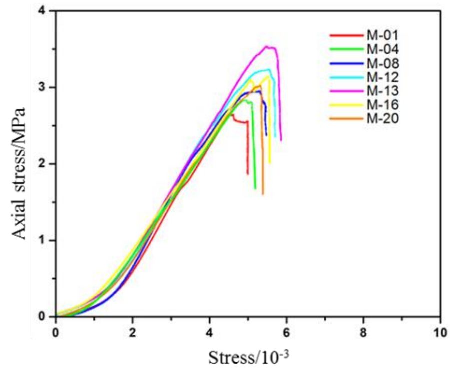

(b) Specimens group M

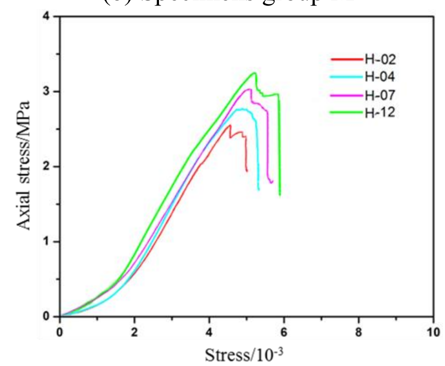

(c) Specimens group H

Fig. 2 Stress-strain curves of rock-like specimens under uniaxial compression

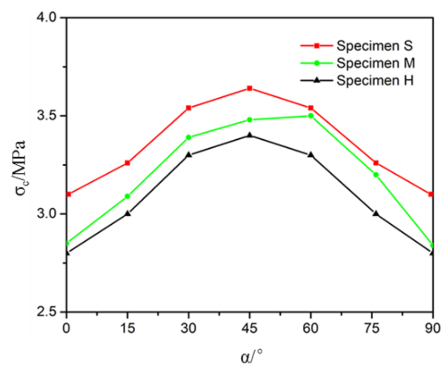

Fig. 3 Variation characteristics of peak stress of specimens with conjugate fractures

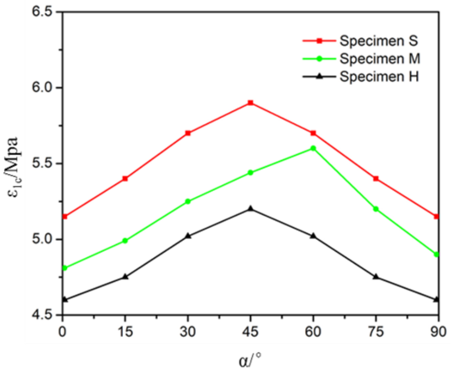

Fig. 4 Variation characteristics of peak axial strain of specimens with conjugate fractures

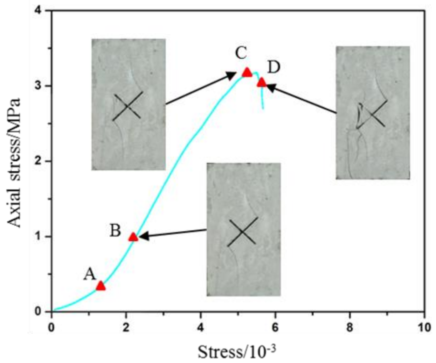

Fig. 5 Crack propagation of M-12 in rock-like specimen

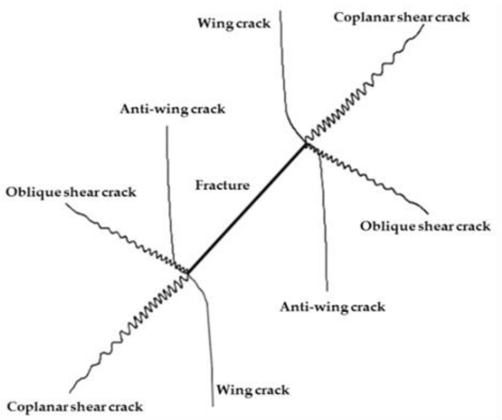

Fig. 6 Crack types of specimen with cracks under uniaxial compression

Fig 4 shows the variation of peak axial strain of rock-like specimens with conjugate fractures at different horizontal angles and fracture lengths. Results show that the peak axial strain intensity increases and then decreases with the increasing horizontal angle α for specimens group S. It reaches a maximum value of 5.92×10^{-3} when the horizontal angle α is 45°. When the horizontal angle increases from 0° to 45°, the peak axial strain intensity increased from 5.15×10^{-3} to 5.92×10^{-3} (14.9% increases). The peak axial strain intensity increases and then decreases with increasing horizontal angle α for specimens group M. It reaches a maximum value of 5.78×10^{-3} when the horizontal angle α is 60°. When the he horizontal angle α increases from 0° to 60°, the peak axial strain intensity increased from 4.77×10^{-3} to 5.78×10^{-3} (21.2% increases). The peak axial strain intensity increases at first and then decreases with the increasing horizontal angle α for specimens group H. It reaches a maximum value of 5.16×10^{-3} when the horizontal angle α is 45°. When the horizontal angle α increases from 0° to 45°, the peak axial strain intensity increased from 4.61×10^{-3} to 5.16×10^{-3} (11.9% increases). With the same horizontal angle α, the peak axial strain gradually decreases with increasing fracture length. For the same main fracture, the axial strain increases at first and then decreases with increasing horizontal angle α.

3.2 Analysis of crack initiation and failure of conjugated fractured rock-like specimens

The relationship between the failure process and stress-strain of the M-12 rock-like specimen is shown in Fig. 5. When the axial stress is applied to point A (σ_1 = 0.62 MPa), the elastic stage starts and the macroscopic surface of the rock-like specimen with conjugate fractures has no crack. With increasing of the axial stress, the elastic stage ends and the plastic stage starts when the point B (σ_1=2.09 MPa) is reached. When reaching the macroscopic behavior of the rock-like strength, as shown by point C (σ_1=3.52 MPa), it enters the failure stage. The tensile crack Tw is generated at the upper and lower tips of the main fracture. When the rock-like specimen reaches the peak of the main fracture respectively sprout secondary fracture, the post-peak stress-strain curve drops sharply to point D (σ_1=3.21 MPa). The upper tip of the secondary fracture and the lower tip of the primary crack create a through-shear crack. Therefore, the rock-like specimen is completely unstable.

4. Comparison between numerical simulation and experiment

4.1 Crack propagation mode

Under uniaxial compression, crack propagation of fractured rock specimens and rock-like specimens varies with the change of horizontal angle and fractures length (Li and Wong 2012, Li and Wong 2014, Zou *et al*. 2016). As the axial stress increases, the crack first initiated at the tip end of the fracture and then propagated along the axial loading direction until the polymerization formed tensile crack of wing crack (Tw) and anti- wing crack (Ta). With the propagation of tensile crack, shear crack of coplanar shear crack (Sc), which is parallel to the fracture and oblique shear crack (So), is generated at the tip as shown in Fig 6. In the uniaxial compression test of specimens with multiple groups of fracture, the cracks are mainly caused by the interaction tensile cracks. The penetration of the rock bridge marks the instability of the specimens (Huang *et al*. 2016, Yang *et al*. 2016, Liu *et al*. 2017).

4.2 Comparative analysis of test and numerical simulation of conjugated fractured rock specimens

To further examine the crack initiation, propagation, failure process and instability characteristics of rock-like

Table 3 Comparison and analysis of uniaxial compression experiment and numerical simulation of specimens group S

Specimen ID	Undamaged	Failure process	Numerical simulation	Sketches
S-02		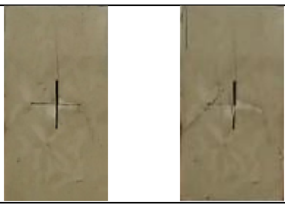	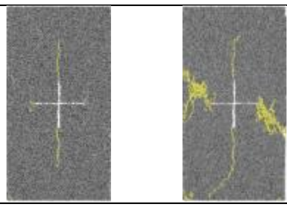	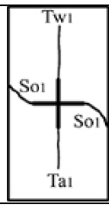
S-05			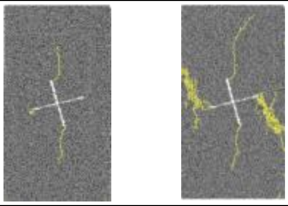	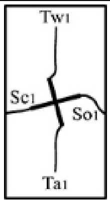
S-07		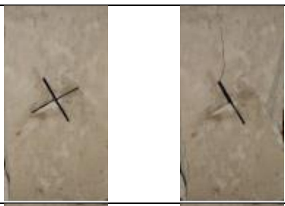	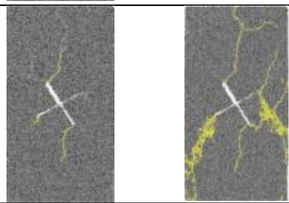	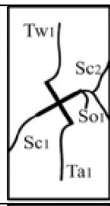
S-11			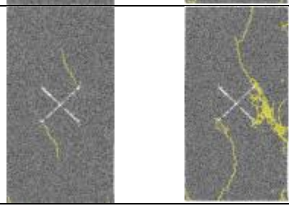	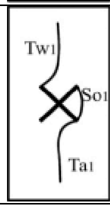

Table 4 Comparison and analysis of uniaxial compression experiment and numerical simulation of specimens group M

Specimen ID	Undamaged	Failure process	Numerical simulation	Sketches
M-01		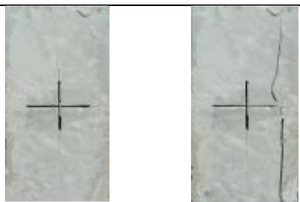	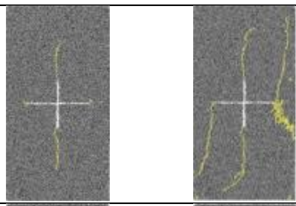	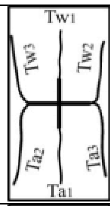
M-04		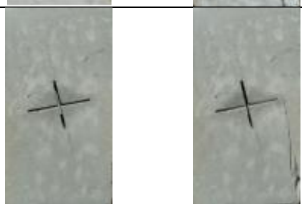	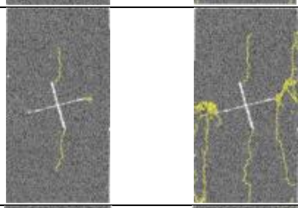	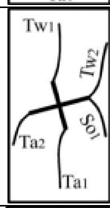
M-08		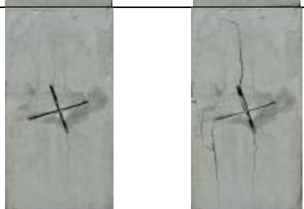	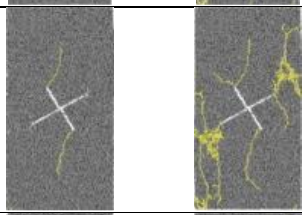	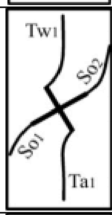
M-12	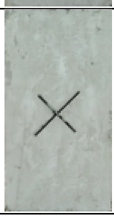	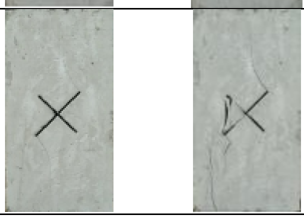	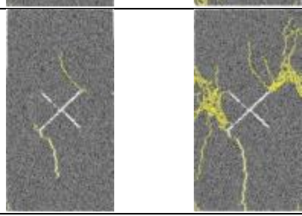	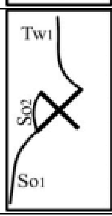

Table 4 Continued

Specimen ID	Undamaged	Failure process	Numerical simulation	Sketches
M-13	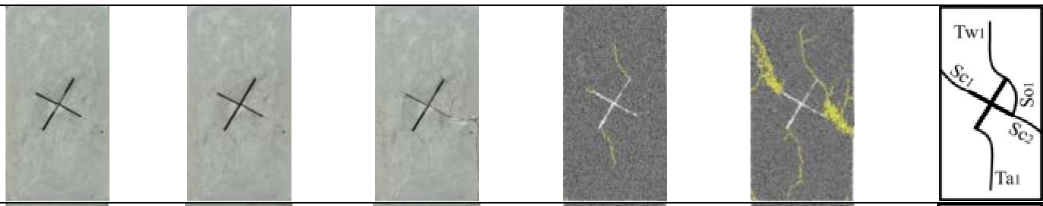			
M-16	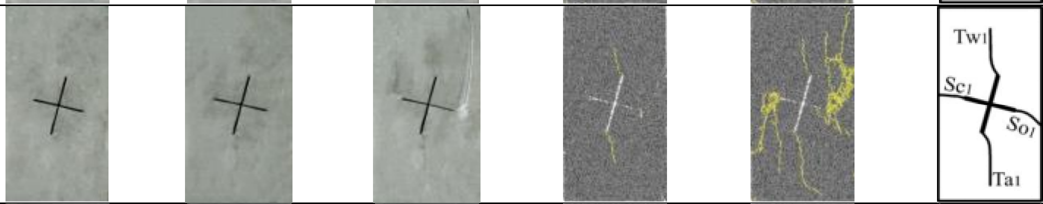			
M-20	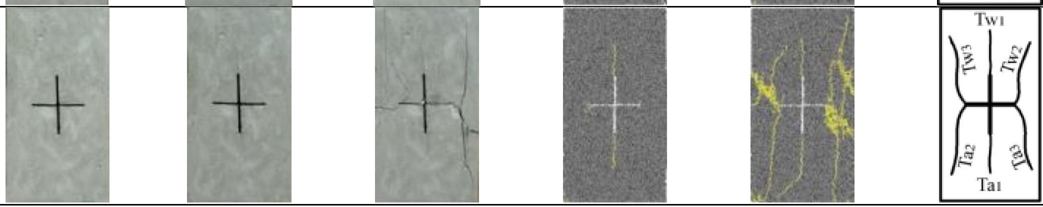			

Table 5 Comparison and analysis of uniaxial compression experiment and numerical simulation of specimens group H

Specimen ID	Undamaged	Failure process	Numerical simulation	Sketches
H-02	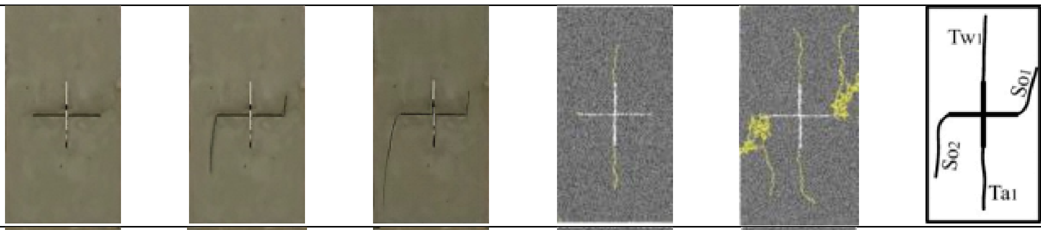			
H-04				
H-07	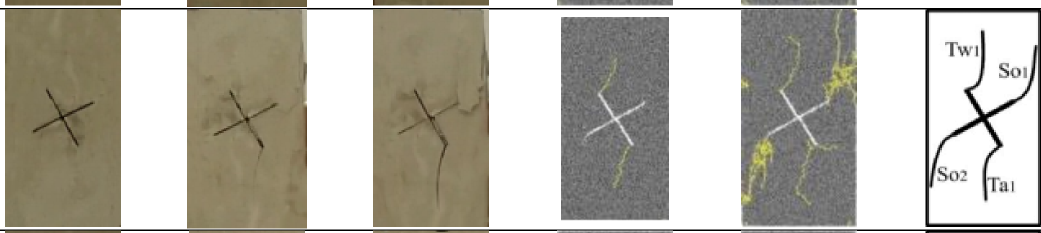			
H-12	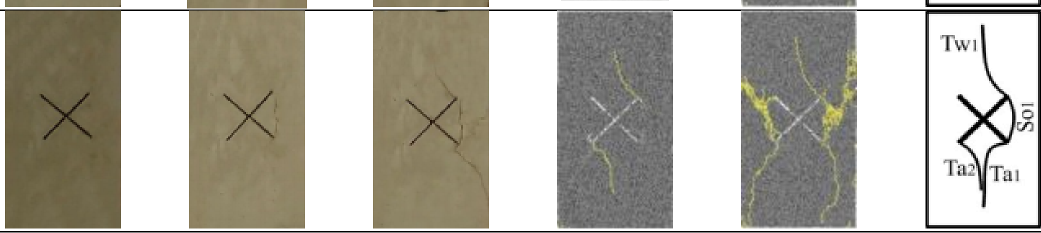			

specimen with conjugated fractures of different horizontal angles and fracture lengths under uniaxial compression, the initiate location of tensile cracks and shear cracks were analyzed and compared for simulation and experimental results. Together with crack distribution sketch, effects of horizontal angle and fracture length on crack initiation and propagation are examined.

As shown in Table 3, for the S-02 specimen with the horizontal angle α of 0°, the main fracture is perpendicular to the loading direction while the secondary fracture is horizontal with the loading direction. With the loading of axial stress, micro cracks propagate in the stress concentration region at the upper tip of the secondary fracture, forming Tw1 in the opposite direction of loading.

Subsequently, crack So_1 appears at the right tip of the main fracture and Sc_1 appears at the left tip of the main fracture. Both extend towards the loading direction. As the loading stress increases, a downward extending of Ta_1 appears at the lower tip of the secondary crack. The crack propagation for S-05 specimen is similar to the S-02 specimen. The shear effect of S-05 specimen is stronger than that for S-02 specimen. Table 4 lists typical crack initiation and propagation diagrams of specimen group M for laboratory experiments and numerical simulation, as well as the final damage sketch.

For specimen S-11 with the horizontal angle α of 45°, with the loading of axial stress, the micro cracks first propagate in the stress concentration region at the upper tips in the direction of loading and lower tips of the secondary fracture in the opposite direction. The cracks then extend to form Tw_1 and Ta_1. Compared with specimen S-07, the upper tip of the main fracture and the lower tip of the secondary fracture form a shear penetration to form So_1 more obviously. Specimen S-07 formed So_1 while So_2 expanded in the opposite direction of loading and formed a clipping region with Sc_1.

Due to different lengths of main fracture and secondary fracture in specimen group M, crack initiation, propagation and coalescence show the differences at the same horizontal angle α for specimens group S and specimens group H. Crack propagation for specimen M-01 and M-20 show the similarity. For both specimens, Tw_1 and Ta_1 appear respectively at the upper and lower tips of the secondary fracture. Tw_2, Tw_3 and Ta_2, Ta_3 appear at the upper and lower tips of the main fracture respectively with the increase of axial loading stress. For specimen M-0 and M-16, when horizontal angle α increases to 15° and 75°, Tw_1 and Ta_1 initiated at the upper and lower tips of the secondary fracture and propagated toward the loading direction. Shear cracks begin to appear at the tip of the main fracture and So_1 appears at the upper tip. At the same time, Sc_1 appears at the lower tip of specimen M-04. When the horizontal angle α increases to 30°, the macro surface shear crack of the specimen increases, Tw_1 and Ta_1 appear at the upper tip and the lower tip of the secondary fracture for specimen M-08. Difference observed for specimen M-04 is that So_1 and So_2 are observed at the upper tip and the lower tip of the main fracture.Tw_1 and Ta_1 appear at the upper tip and the lower tip of the secondary fracture for specimen M-08. Difference observed for specimen M-04 is that So_1 and So_2 are observed at the upper tip and the lower tip of the main fracture.

When the horizontal angle α is 45°, specimen M-12 differs with other specimens in the length of the fracture. With the increase of axial stress, secondary fracture formed Tw_1; So_1 formed at the lower tip; and So_2 formed in the main fracture upper tip and the secondary fracture lower tip. For specimen M-13, main fracture is more parallel to the loading direction than that of specimen M-12. With combining effects from horizontal angle α and fractures length L, the crack first appeared at the upper and lower tips of the main fracture to form Tw_1 and Ta_1. As the axial loading stress increases, Sc_1 and Sc_2 appear simultaneously at the upper and lower tips of the secondary fracture, while the primary fracture at the upper tip of and the secondary fracture at the lower tip form So_1.

Specimens group H listed in Table 5 are the same as specimens group S listed in Table 3 under the same horizontal angle α. The main fracture and the secondary fracture are longer for specimens group H than specimens group S. Cracks are initiated and destructed at an earlier time. For specimens group H, shear cracks at the same horizontal angle are easier to be generated and they propagated and formed shear zones.

5. Conclusions

(1) By comparing the peak strength of rock-like specimens with different horizontal angles under the same main fracture and secondary fracture lengths, it was found that with the increase of horizontal angle α, the peak strength first increases and then decreases. The maximum strength of specimen group S and specimen group H is observed at the horizontal angle of 45°. The maximum strength of specimen group M is at the horizontal angle of 60°. Comparing peak strength of different main fracture and secondary fracture lengths under horizontal angle α, it is concluded that the peak strength decreases gradually with the increase of fracture length. This indicates that horizontal angle and fracture length have certain influence on the peak strength of the specimens.

(2) Under the same length of the main and secondary fractures, the peak axial strain increases at first and then decreases with increase of horizontal angle α. For both specimens group S and specimens group H, the maximum peak axial strain is reached when the horizontal angle is 45°. For specimens group M, the maximum peak stress axial strain is reached at a horizontal angle of 60°. Results show that the peak axial strain gradually increases with the increase of the fracture length.

(3) Analysis of cracks initiation, propagation and coalescence shows large differences with the change of horizontal angle α and fractures length. For specimens group S and specimens group H, when horizontal angle increases from 0° to 30°, the shear crack is gradually strengthened at the tip of the main fracture. The penetrating shear crack appears at the same time when the horizontal angle is 45°. Specimens group M showed different lengths of main fracture and the secondary fracture. The penetrating shear cracks occur at a horizontal angle of 60° is more obvious, compared to that when the horizontal angel is 45°.

(4) When the horizontal angle of specimens group S and specimens group M increases from 0° to 45°, the upper and lower tips of the secondary fracture generated Tw and To, propagating in the loading direction and the opposite direction of loading, respectively. When the horizontal angle of specimens group H increases from 0° to 45°, the upper and lower tips of the secondary fracture generated Tw and To, propagating in the loading direction and the opposite direction of loading, respectively. When the horizontal angle increases from 45° to 90°, the upper and lower tips of the main fracture generated Tw and To, propagating in the loading direction and the opposite

direction of loading, respectively.

Acknowledgements

This research was financially supported by the National Natural Science Foundation of China (Grant No.51404146), China Postdoctoral Science Foundation (Grant No.2015M572067), Postdoctoral Innovation Project of Shandong Province (Grant No. 152799),Qingdao Postdoctoral Applied Research Project (Grant No.2015203), AnHui Province Key Laboratory of modern mining engineering Foundation (Grant No. KLMME12101), the SDUST Research Fund (grant 2018TDJH102), the Young Teachers' Growth Program of Shandong Province.

References

Bagheripour, M., Rahgozar, R. and Pashnesaz, H. (2011), "A complement to Hoek-Brown failure criterion for strength prediction in anisotropic rock", *Geomech. Eng.*, **3**(1), 61-81.

Cai, P., Nie, W., Chen, D.W., Yang, S.B. and Liu, Z.Q. (2019), "Effect of air flowrate on pollutant dispersion pattern of coal dust particles at fully mechanized mining face based on numerical simulation", *Fuel*, **239**, 623-635.

Cao, R., Cao, P. and Lin, H. (2017), "Experimental and numerical study of the failure process and energy mechanisms of rock-like materials containing cross unpersistent joints under uniaxial compression", *Plos One*, **12**(12), e0188646.

Da Silva, B.G. and Einstein, H.H. (2013), "Modeling of crack initiation, propagation and coalescence in rocks", *Int. J. Fract.*, **182**(2), 167-186.

Erarslan, N. (2016), "Microstructural investigation of subcritical crack propagation and fracture process zone (FPZ) by the reduction of rock fracture toughness under cyclic loading", *Eng. Geol.*, **208**, 181-190.

Fu, J., Zhang, X. and Zhu, W. (2017), "Simulating progressive failure in brittle jointed rock masses using a modified elastic-brittle model and the application", *Eng. Fract. Mech.*, **178**, 212-230.

Haeri, H., Khaloo, A. and Marji, M.F. (2015), "Experimental and numerical simulation of the microcrack coalescence mechanism in rock-like materials", *Strength Mater.*, **47**(5), 740-754.

Haeri, H., Shahriar, K. and Marji, M.F. (2014), "Experimental and numerical study of crack propagation and coalescence in pre-cracked rock-like disks", *Int. J. Rock Mech. Min. Sci.*, **67**, 20-28.

Huang, Y., Yang, S. and Tian, W. (2016), "An experimental study on fracture mechanical behavior of rock-like materials containing two unparallel fissures under uniaxial compression", *Acta. Mech. Sinica*, **32**(3), 442-455.

Jin, J., Cao, P. and Chen, Y. (2017), "Influence of single flaw on the failure process and energy mechanics of rock-like material", *Comput. Geotech.*, **86**, 150-162.

Komurlu, E., Kesimal, A. and Demir, S. (2016), "Experimental and numerical analyses on determination of indirect (splitting) tensile strength of cemented paste backfill materials under different loading apparatus", *Geomech. Eng.*, **10**(6), 775-791.

Kong, B., Li, Z., Wang, E., Lu, W., Chen, L. and Qi, G. (2018), "An experimental study for characterization the process of coal oxidation and spontaneous combustion by electromagnetic radiation technique", *Proc. Safety Environ. Protect.*, **119**, 285-294.

Lee, H. and Jeon, S. (2011), "An experimental and numerical study of fracture coalescence in pre-cracked specimens under uniaxial compression", *Int. J. Solids Struct.*, **48**(6), 979-999.

Li, H. and Wong, L. (2012), "Influence of flaw inclination angle and loading condition on crack initiation and propagation", *Int. J. Solids Struct.*, **49**(18), 2482-2499.

Li, H. and Wong, L. (2014), "Numerical study on coalescence of Pre-Existing flaw pairs in Rock-Like material", *Rock Mech. Rock. Eng.*, **47**(6), 2087-2105.

Liu, Y., Dai, F. and Fan, P. (2017), "Experimental investigation of the influence of joint geometric configurations on the mechanical properties of intermittent jointed rock models under cyclic uniaxial compression", *Rock Mech. Rock. Eng.*, **50**(6), 1453-1471.

Lu, Y., Wang, L. and Elsworth, D. (2015), "Uniaxial strength and failure in sandstone containing a pre-existing 3-D surface flaw", *Int. J. Fracture*, **194**(1), 59-79.

Panaghi, K., Golshani, A. and Takemura, T. (2015), "Rock failure assessment based on crack density and anisotropy index variations during triaxial loading tests", *Geomech. Eng.*, **9**(6), 793-813.

Sarfarazi, V., Haeri, H., Marji, M.F. and Zhu, Z.M. (2017), "Fracture mechanism of brazilian discs with multiple parallel notches using PFC2D", *Polytech. Civ. Eng.*, **61**(4), 653-663.

Shen, B. and Barton, N. (2018), "Rock fracturing mechanisms around underground openings", *Geomech. Eng.*, **16**(1), 35-47.

Sun, X.Z., Shen, B. and Zhang, B.L. (2018), "Experimental study on propagation behavior of three-dimensional cracks influenced by intermediate principal stress", *Geomech. Eng.*, **14**(2), 195-202.

Wang, G., Wu, M., Wang, R., Xu, H. and Song, X. (2017), "Height of the mining-induced fractured zone above a coal face", *Eng. Geol.*, **216**, 140-152.

Wang, S.Y., Sloan, S.W. and Sheng, D.C. (2014), "Numerical study of failure behaviour of pre-cracked rock specimens under conventional triaxial compression", *Int. J. Solids Struct.*, **51**(5), 1132-1148.

Wang, X. and Tian, L. (2018), "Mechanical and crack evolution characteristics of coal-rock under different fracture-hole conditions: A numerical study based on particle flow code", *Environ. Earth. Sci.*, **77**(8), 297.

Yang, L., Jiang, Y. and Li, S. (2013), "Experimental and numerical research on 3D crack growth in rocklike material subjected to uniaxial tension", *J. Geotech. Geoenviron. Eng.*, **139**(10), 1781-1788.

Yang, S., Jing, H. and Xu, T. (2014), "Mechanical behavior and failure analysis of brittle sandstone specimens containing combined flaws under uniaxial compression", *J. Central South Univ.*, **21**(5), 2059-2073.

Yang, S., Tian, W. and Huang, Y. (2016), "An experimental and numerical study on cracking behavior of brittle sandstone containing two non-coplanar fissures under uniaxial compression", *Rock Mech. Rock Eng.*, **49**(4), 1497-1515.

Zhang, X., Liu, Q. and Wu, S. (2015), "Crack coalescence between two non-parallel flaws in rock-like material under uniaxial compression", *Eng. Geol.*, **199**, 74-90.

Zhao, X.G., Cai, M. and Wang, J. (2015), "Objective determination of crack initiation stress of brittle rocks under compression using AE measurement", *Rock Mech. Rock Eng.*, **48**(6), 2473-2484.

Zhou, X., Zhang, J. and Wong, L. (2018), "Experimental study on the growth, coalescence and wrapping behaviors of 3D cross-embedded flaws under uniaxial compression", *Rock Mech. Rock Eng.*, **51**(5), 1379-1400.

Zhou, X.P., Bi, J. and Qian, Q.H. (2015), "Numerical simulation of crack growth and coalescence in rock-like materials containing multiple pre-existing flaws", *Rock Mech. Rock Eng.*, **48**(3), 1097-1114.

Zou, C., Wong, L.N.Y. and Loo, J.J. (2016), "Different mechanical and cracking behaviors of single-flawed brittle gypsum specimens under dynamic and quasi-static loadings", *Eng*. *Geol*., **201**, 71-84.

CC